On C^0 and C^1 continuity of envelopes of rotational solids and its application to 5-axis CNC machining

Felipe Ponce-Vanegas[1], Michal Bizzarri[1,2], and Michael Bartoň[1,3]

[1]Basque Center for Applied Mathematics
[2]Department of Mathematics, Faculty of Applied Sciences, University of West Bohemia
[3]Ikerbasque – Basque Foundation for Sciences

Abstract

We study the smoothness of envelopes generated by motions of rotational rigid bodies in the context of 5-axis Computer Numerically Controlled (CNC) machining. A moving cutting tool, conceptualized as a rotational solid, forms a surface, called envelope, that delimits a part of 3D space where the tool engages the material block. The smoothness of the resulting envelope depends both on the smoothness of the motion and smoothness of the tool. While the motions of the tool are typically required to be at least C^2, the tools are frequently only C^0 continuous, which results in discontinuous envelopes. In this work, we classify a family of instantaneous motions that, in spite of only C^0 continuous shape of the tool, result in C^0 continuous envelopes. We show that such motions are flexible enough to follow a free-form surface, preserving tangential contact between the tool and surface along two points, therefore having applications in shape slot milling or in a semi-finishing stage of 5-axis flank machining. We also show that C^1 tools and motions still can generate smooth envelopes.

1 Introduction

Geometric modeling of manufacturing processes such as multi-axis Computer Numerical Controlled (CNC) machining has been a very active research area of Computer Aided Geometric Design (CAGD) since its inception in the late 60s and has attracted many researchers over the past several decades; see *e.g.* [12, 15, 6, 18, 16, 17, 3] and other relevant references cited therein. While the case of 3-axis CNC machining is rather simple from the kinematic point of view, as the instantaneous motion is always a pure translation, the motion planning in the case of 5-axis is a lot more challenging as the instantaneous motion is a general *helical motion* (also known as *screw* motion); see [14].

Figure 1: A complex cutting tool whose meridian contains several points of only C^0 continuity.

We study the smoothness of envelopes generated by the motions of rotational rigid bodies (rotational solids). Even though the theory of envelopes is old and has important industry applications, there is, to the best of our knowledge, a gap in the literature about the smoothness of envelopes. Our motivation comes from the application of 5-axis *flank* (also known as side) CNC milling and/or shape slot milling of curved, free-form objects, where the tool moves sideways along a reference surface and therefore touches it tangentially at (theoretically) infinitely many points, i.e., along a curve called *characteristic*.

Even though the cutting tool is not exactly a rotational solid — it contains flutes or bumps, and also holes for cooling fluid like in Fig. 1 — the tool spins around its axis at high speed compared to the feed rate, and therefore one conceptualizes the tool as a *solid of revolution*. The motion of the tool in 3D space forms, typically, a pair of surfaces[1] called *envelopes*; see Fig. 2. One envelope branch is usually irrelevant for machining purposes, but the envelope closer to the reference surface should approximate it very well, and one can therefore interpret the motion-planning of 5-axis flank CNC machining as an approximation problem.

The final smoothness of the envelope is governed by the smoothness of the tool and the motion. If the shape of the tool and the motion are both C^2 continuous, that is, if they have second derivatives continuous everywhere, then the envelope is only C^1-continuous *locally*. This comes from the fact that the construction of the envelope involves a time derivative, so one loses one derivative and drops from C^2 to C^1. We stress the word "locally" because the envelope may have self-intersections, but if we restrict ourselves to a small time interval, and a small height interval in the tool, then the envelope will be a C^1-surface in the usual sense. This is a classical result that we recall in Theorem 3; see, *e.g.*, [9, Theorem 85.1].

The general rule is that a C^k-tool and -motion generates envelopes with C^{k-1} characteristic curves. For example, in the case of C^1-tool and -motion, the characteristic curves have sharp corners, nevertheless, the envelope remains surprisingly C^1; see Section 3. On the other hand, for C^0-tools the envelope does not enjoy such persistence of smoothness; see Fig. 3.

When the tool is only C^0 continuous, the envelope is in general discontinuous and can contain internal gaps, which is very undesirable in the context of machining; see Fig. 3 (b).

---

[1]Algebraically, an envelope is a single surface, which may have two real branches; however, in engineering literature, one typically speaks about two (upper and lower) envelopes.
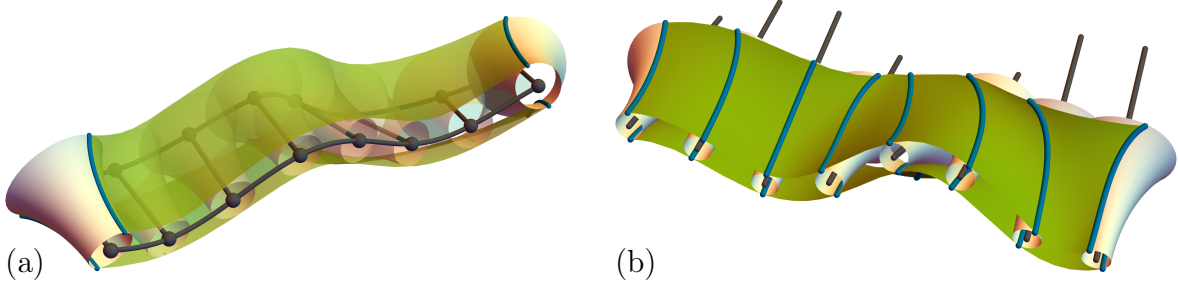
Figure 2: (a) A rigid body motion of a rotational tool forms an envelope (green) that typically has two branches. The motion is fully determined by the motion of the tool axis (dark bold). (b) At each time instant, the tool touches the envelope along a characteristic curve (blue). Notice that the characteristic is not a static curve, but changes dynamically during the motion.
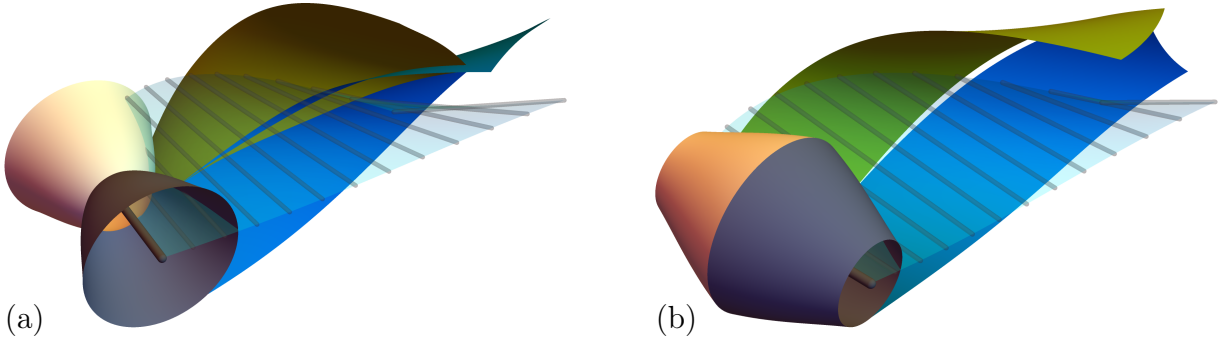

Figure 3: Generic motions with C^0 tools produce discontinuous envelopes: (a) concave profiles generate intersecting envelopes, while (b) convex profiles generate gapped envelopes. The ruled surfaces (transparent blue) visualize the motion of the tool, which is C^2, yet the resulting envelope is discontinuous.

One naturally raises a question if this drop of continuity is something that always happens, and if not, which conditions prevent it from happening; see Sec. 4. In this work we study the problem of envelope continuity and formulate conditions on the motion of the tool that guarantee preservation of the continuity.

In our first result, whose precise statement we delay to Section 3, we study what happens when the regularity drops one derivative at some points.

Theorem A. *If the tool and the motion are globally C^1 but only piecewise C^2, then the envelope is still a C^1-surface locally away from the edge of regression.*

An immediate consequence of Theorem A is that the tool and the motion can be designed using only C^1 quadratic splines and still get a regular surface.

Before stating the next result, we need additional background. To describe the motion of the tool, one can select velocity vectors at two points, typically (but not necessarily) the endpoints of the axis; one has 2×3 degrees of freedom (DoFs). Since the instantaneous

3

motion is defined up to a scalar multiple, one can further assume that one vector is unit (5 DoFs). But the two vectors are bind together by the projection rule, i.e., their projections on the axis is the same oriented distance, see e.g. [5, Eq. (15)]. Otherwise, the vector field defined by the two vectors does not correspond to a motion of a rigid body (axis of the tool). Consequently, one ends up with *four degrees of freedom*. The other vectors of the velocity field are obtained by interpolation; for more detailed explanation see, e.g., [14, Chapter 3.4.1].

Now consider a tool having only piecewise C^1 continuous meridian, that is, the meridian curve contains a finite set of C^0 discontinuities (cusps). One can still design the motions so that the envelope remains continuous, but each cusp reduces the number of degrees of freedom (at each time instant) by one, and since the tool is required to move tangentially along the input surface, the only practical scenario is the case with a single cusp.

Theorem B. *If the tool is piecewise C^1, and the derivative is discontinuous only at a single point, then at every time there are three degrees of freedom to move the tool so that the envelope is C^0.*

Interestingly enough, when passing from C^2-tool and -motion to C^1, the envelope remains C^1, but for C^0-tool the envelope becomes discontinuous; it does not go through an intermediate C^0-stage.

Necessary and sufficient conditions for envelopes to be G^1 in multi-pass flank milling are presented in [19]. In terms of the tool regularity, the reader is referred *e.g.* to [10]. There are several related works that deal with computing motions of rigid bodies, both in 2D and 3D. In particular, one can describe envelope singularities in 2D [7], detect self-intersections of free-form curves and surfaces [13], or sweeps of rigid bodies [1], or efficiently calculate swept volumes of rigid bodies [4]. In the context of 5-axis CNC machining, there are works on motion modeling of piece-wise C^1 cutters via Gauss maps [10, 11], path-planning algorithms with toroidal [15, 3] and barrel [12] cutters, motion smoothing [18, 8], or motion approximation [16, 17]. However, the full classification of motions that can still generate continuous envelopes with only C^0-continuous tools is, to the best of our knowledge, missing.

The rest of the paper is organized as follows: Section 2 briefly recalls the classical theory of rigid body motions and envelopes. In Section 3 we prove Theorem A, and in Section 4 prove Theorem B. We show some examples in Section 4.3 and conclude the paper in Section 5.

2   Preliminaries

In this Section we recall some basic facts about rigid bodies and their envelopes. A moving rigid body in 3D can be represented as the zero set of a multivariate scalar function $G(\mathbf{x}, t) = 0$, where $\mathbf{x} \in \mathbb{R}^3$ is a point in 3D space and t can be interpreted as time (or pseudo-time). Let us consider in more generality a family of functions $G(\mathbf{x}, t) : \mathbf{x} \in \mathbb{R}^3 \to \mathbb{R}$ parameterized by $t \in \mathbb{R}$, so that the functions $G(\cdot, t)$ define a family of surfaces $S_t := \{\mathbf{x} : G(\mathbf{x}, t) = 0\}$.

A surface Ω that touches tangentially the one parameter family of surfaces S_t is called an *envelope*. The fact the envelope touches each S_t corresponds to a constraint that the time

derivative of G vanishes at the contact point of Ω and S_t. Therefore, the locus of the contact points $\mathbf{x}$ is described as

$$G(\mathbf{x}, t) = \partial_t G(\mathbf{x}, t) = 0 \qquad t \in I. \tag{1}$$

At a fixed time instant $t \in I$, Eq. (1) is an intersection of two hypersurfaces in $\mathbb{R}^3$ and therefore generically a one-dimensional entity known as a *characteristic curve*; notice that the vectors $\nabla_{\mathbf{x}} G \times \nabla_{\mathbf{x}} \partial_t G$ are tangent to the characteristic curves.

Generically, the points $\mathbf{x} \in \mathbb{R}^3$ where

$$G(\mathbf{x}, t) = \partial_t G(\mathbf{x}, t) = \partial_t^2 G(\mathbf{x}, t) = 0 \qquad \text{as } t \text{ runs through some interval,} \tag{2}$$

form a curve called the *edge of regression*; in some cases this curve may degenerate into a set of points. At a fixed time instant t, Eq. (2) gives a finite set of points, so by varying t we get generically a curve. The edge of regression itself is an envelope of the family of characteristic curves [9, Theorem 85.2], and the envelope Ω is prone to develop a singularity along it, as Example 2 shows. Therefore, to guarantee smoothness, one needs to stay sufficiently far away from the edge of regression. Before formulating it as a theorem for envelopes in 3D, we demonstrate the situation first in a 2D analogue, which can be better visualized. Note that for the 2D analogy, we consider a family of planar curves, and the envelope is again a curve.

Example 1. *Smooth envelope. In Fig. 4(a) we consider a one-parameter family of lines $G = x_1 + x_2 t + t^2 = 0$ in a (x_1, x_2)-plane, t being the parameter of the family. The family can be seen as a hypersurface (a quadric) in $\mathbb{R}^2 \times \mathbb{R}$; see Fig. 4(a). Differentiating G yields $\partial_t G = x_2 + 2t$, which is linear and its zero set corresponds to the blue plane in Fig. 4(a). The 3D curve $\tilde{\Omega}$ is the intersection of $G = 0$ and $\partial_t G = 0$, and its projection to the (x_1, x_2)-plane gives the desired envelope Ω. Fig. 4(a) bottom framed shows the top view (an orthogonal projection into the (x_1, x_2)-plane in the direction t), where $\tilde{\Omega}$ projects into Ω, and the rulings of the $G = 0$ system envelop it.*

Now consider the situation at the origin at time $t = 0$, that is, $(\mathbf{x}_0, t_0) = (\mathbf{0}, 0)$. The gradients of G and $\partial_t G$ are $\nabla_{(\mathbf{x},t)} G(0) = [1, 0, 0]$ and $\nabla_{(\mathbf{x},t)} \partial_t G(0) = [0, 1, 2]$, respectively; see Fig. 4(a). Since $\partial_t^2 G \neq 0$, then the projection of $\tilde{\Omega}$ around $\mathbf{0}$ has a well-defined tangent line.

Example 2. *Edge of regression. In Fig. 4(b) we consider a one-parameter family of lines $G = x_1 + x_2 t + t^3 = 0$ in the (x_1, x_2)-plane. The analysis is similar to that in Example 1, however, $\partial_t G = x_2 + 3t^2$ is a degenerate quadric (blue surface in Fig. 4(b)).*

Now, at $(\mathbf{x}_0, t_0) = (\mathbf{0}, 0)$, the gradients of G and $\partial_t G$ are $\nabla_{(\mathbf{x},t)} G(0) = [1, 0, 0]$ and $\nabla_{(\mathbf{x},t)} \partial_t G(0) = [0, 1, 0]$, respectively; for visualization purposes, we plot in blue $-\nabla_{(\mathbf{x},t)} \partial_t G(0)$, to make it better visible. In this case $\partial_t^2 G(0) = 0$, so the curve $\tilde{\Omega}$ is parallel to the t axis at $(\mathbf{0}, 0)$ and its projection to the (x_1, x_2)-plane contains a cusp. The projection is again displayed bottom framed, showing the cusp of Ω at $[0, 0]$.

Theorem 3. *Let G and $\partial_t G \in C^1(\mathbb{R}^3 \times \mathbb{R})$. Assume that $\mathbf{x}_0 \in \Omega$ satisfies Eq. (1) for some $t_0 \in \mathbb{R}$. If $\nabla_{\mathbf{x}} G(\mathbf{x}_0, t_0)$ and $\nabla_{\mathbf{x}} \partial_t G(\mathbf{x}_0, t_0)$ are linearly independent and $\partial_t^2 G(\mathbf{x}_0, t_0) \neq 0$, then Ω is a C^1-surface in a neighborhood of $\mathbf{x}_0$ and Ω touches*

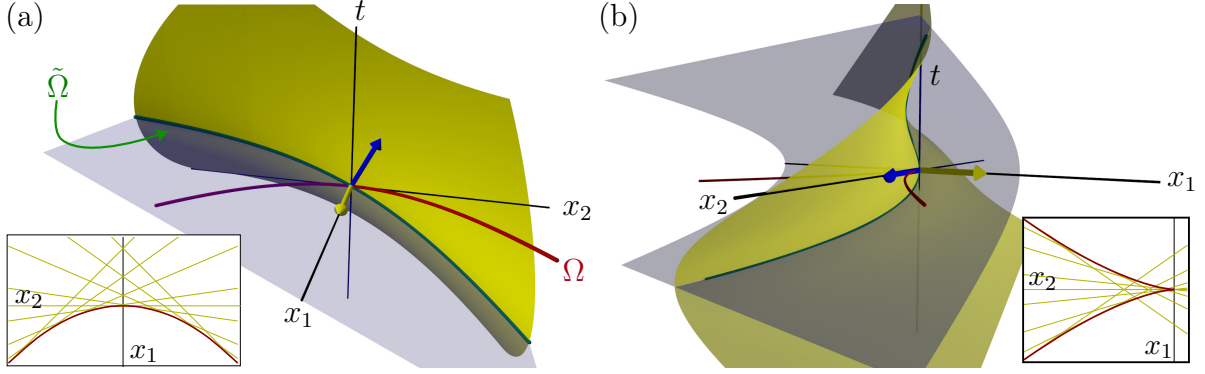$$S_t := \{\mathbf{x} : G(\mathbf{x}, t) = 0\}$$

Figure 4: A 2D analogue of Theorem 3 visualized in $\mathbb{R}^2 \times \mathbb{R}$. Considering time as the vertical t-axis, a one-parameter family of curves $G = 0$ forms a hypersurface in $\mathbb{R}^3$ (yellow). A locus of points (x_1, x_2, t) that solves Eq. (1), $\tilde{\Omega}$, is a 3D curve, and its projection to the (x_1, x_2)-plane is the envelope Ω (red). The gradients $\nabla_{(\mathbf{x},t)}G(0)$ (yellow) and $\nabla_{(\mathbf{x},t)}\partial_t G(0)$ (blue) at $(\mathbf{x}_0, t_0) = (\mathbf{0}, 0)$ are shown. In the small boxes, the views of several discrete lines (yellow) and the envelope Ω (red) are shown. (a) a regular scenario; (b) a cusp.

tangentially for all t in a neighborhood of t_0. Furthermore, we can choose a parameterization $\psi : \mathbb{R}^2 \mapsto \Omega$ so that the curves $u_2 \mapsto \psi(u_1, u_2)$ are characteristics.

Proof. The envelope can be seen as the projection of the set

$$\tilde{\Omega} := \{(\mathbf{x}, t) : G(\mathbf{x}, t) = \partial_t G(\mathbf{x}, t) = 0\}$$

into the $\mathbf{x}$-space in the t-direction; recall Fig. 4 for a 2D representation of the proof with $\mathbf{x} = (x_1, x_2)$. Since $\nabla_{(\mathbf{x},t)}G$ and $\nabla_{(\mathbf{x},t)}\partial_t G$ are linearly independent, then by the Implicit Function Theorem $\tilde{\Omega}$ is a C^1-surface in $\mathbb{R}^3 \times \mathbb{R}$ parameterized by some $\tilde{\psi} = (\tilde{\psi}_1, \tilde{\psi}_2, \tilde{\psi}_3, \tilde{\psi}_4) :$ $\mathbb{R}^2 \to \mathbb{R}^3 \times \mathbb{R}$, so we may take $\psi := (\tilde{\psi}_1, \tilde{\psi}_2, \tilde{\psi}_3)$ as a parameterization of Ω around $\mathbf{x}_0$. Since $\nabla_{(\mathbf{x},t)}G(\mathbf{x}_0, t_0) = (\nabla_{\mathbf{x}}G(\mathbf{x}_0, t_0), 0)$ and $\partial_t^2 G(\mathbf{x}_0, t_0) \neq 0$, then Ω is a smooth surface.

To prove the last claim of Theorem 3, first notice that $\tilde{\psi}_4$ represents the map $t : \Omega \to \mathbb{R}$ that assigns to each $\mathbf{x} \in \Omega$ the value of t for which the identities in Eq. (1) hold, that is, $G(\mathbf{x}, t(\mathbf{x})) = \partial_t G(\mathbf{x}, t(\mathbf{x})) = 0$. Differentiating $\partial_t G = 0$, we can see that the gradient of $\tilde{\psi}_4$ does not vanish. In fact

$$0 = \nabla_{\mathbf{x}}\partial_t G \cdot \nabla_{\mathbf{u}}\psi + \partial_t^2 G \nabla_{\mathbf{u}}\tilde{\psi}_4, \tag{3}$$

and we can always choose $\mathbf{u} = (u_1, u_2)$ so that the first inner product is different from zero, from which $\nabla_{\mathbf{u}}\tilde{\psi}_4 \neq 0$. Hence, we can always redefine $\tilde{\psi}$ so that $\tilde{\psi}_4(u_1, u_2) = u_1$. Since $\partial_2 \tilde{\psi}_4 = 0$ when $\tilde{\psi}_4 = u_1$, then Eq. (3) implies that $\partial_2 \psi$ is orthogonal to $\nabla_{\mathbf{x}}\partial_t G$, so $u_2 \mapsto \psi(u_1, u_2)$ is a characteristic curve; we may think of u_1 as t.

To see that Ω touches each S_t around t_0 tangentially, differentiate $G(\psi(\mathbf{u}), u_1) = 0$. $\square$

In the remainder of this section we derive a natural parameterization for the envelope; see also [20]. Since the application in mind is 5-axis flank milling, we consider rotational solids

as our moving bodies. Recall that at time t the solid is delimited by a surface $G(\mathbf{x}, t) = 0$. It is convenient to represent the tool in a canonical position as the zero set of the function

$$F(\mathbf{y}) := \frac{1}{2}(r(y_3)^2 - |(y_1, y_2)|^2), \qquad \text{for} \ -L/2 \leq y_3 \leq L/2,$$

where $r > 0$ are the radii of the orbit circles on the tool, and L is the length of the tool. We usually replace y_3 by h, which stands for the height; see Fig. 5(a).
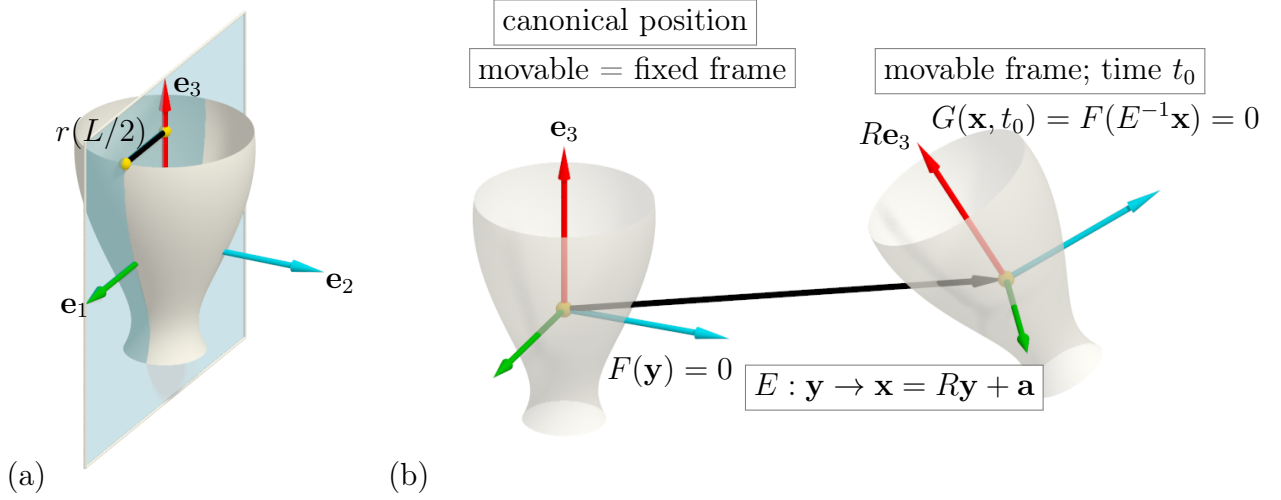

(a)   (b)

Figure 5: Congruent mapping of a surface of revolution. (a) A rotational surface with the axis $\mathbf{e}_3$ is determined by a univariate function r that for each point on the axis assigns a distance (radius of the circle). The tool is delimited by two horizontal planes: $y_3 = \pm L/2$; the radius $r(L/2)$ is shown in black. (b) In the canonical position, fixed frame coincides with the movable frame, that is, E is identity. The movable frame gets transformed via the mapping E. The implicit equation $F(\mathbf{y}) = 0$ with respect to the movable frame remains unchanged, while with respect to the fixed frame the implicit equation is transformed via the rigid body motion E, which is controlled by the rotation matrix R and the translation vector $\mathbf{a}$ (black) that maps the origin to a new position.

Remark 1. *In rigid body kinematics, one typically uses two frames, fixed and movable; see Fig. 5(b). We will use the symbol $\mathbf{y}$ for points with coordinates expressed with respect to the movable frame and $\mathbf{x}$ for points related to the fixed frame. Analogously, we use F and G for implicit equations with respect to the movable and fixed frame, respectively.*

The motion of the tool using Euclidean transformations is represented as

$$E\mathbf{y} := R\mathbf{y} + \mathbf{a}, \qquad \text{where } \mathbf{a} \in \mathbb{R}^3 \text{ and } R \in SO(3) \text{ is a rotation.}$$

If $R(t)$ satisfies $R(0) = I$, then $\frac{d}{dt}R(0)\mathbf{y} = \omega \times \mathbf{y}$, where ω is the angular velocity, that is, a vector along the axis of instantaneous rotation and magnitude equal to the rate of rotation;

see Fig. 6(a). More explicitly,

$$\tfrac{d}{dt}R\mathbf{y} = \omega \times \mathbf{y} = \begin{pmatrix} 0 & -\omega_3 & \omega_2 \\ \omega_3 & 0 & -\omega_1 \\ -\omega_2 & \omega_1 & 0 \end{pmatrix} \begin{pmatrix} y_1 \\ y_2 \\ y_3 \end{pmatrix}.$$

In general, we define $\omega(t)$ by $\omega(t) \times \mathbf{y} := R^T \tfrac{d}{dt}R\mathbf{y}$ (recall that $R^T = R^{-1}$), so the tool is rotating around the axis $R\omega$. Notice that $R\mathbf{e}_3$ is a unit vector aligned with the tool axis, so $\tfrac{d}{dt}R\mathbf{e}_3 = R\omega \times R\mathbf{e}_3$ is the velocity of rotation of the tool axis; see Fig. 6.
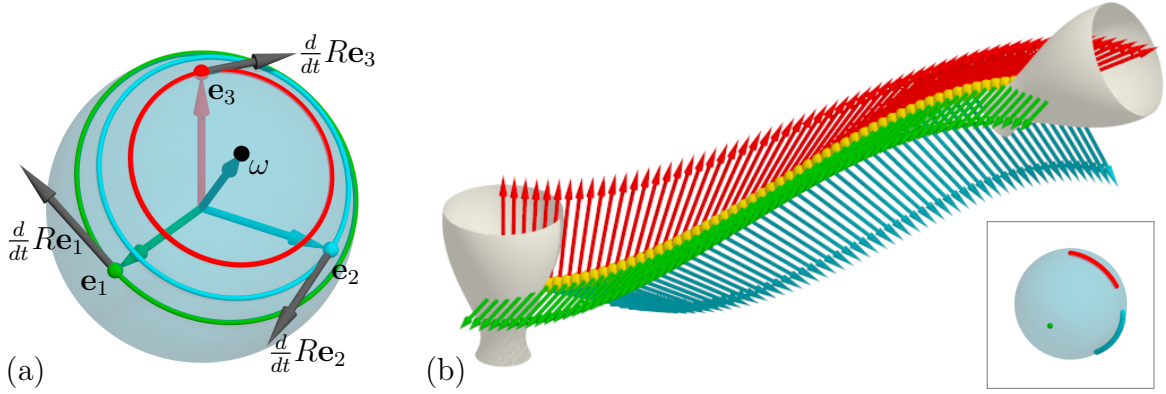

(a)   (b)

Figure 6: Instantaneous velocity. (a) A rotation R of a unit sphere (transparent) for an angular momentum $\omega = (\omega_1, \omega_2, \omega_3)$, (here $\|\omega\| = 1$). The endpoints of the unit vectors on the orthonormal frame $\{\mathbf{e}_1, \mathbf{e}_2, \mathbf{e}_3\}$ travel along the orbits, with the instantaneous velocities $\tfrac{d}{dt}R\mathbf{e}_i$, $i = 1, 2, 3$. (b) A rigid body motion of a rotational solid (light) is determined by the rotational component $\omega(t)$ and translation of the origin, $\mathbf{a}(t)$ (yellow). The rotation of the frame on the unit sphere is shown (bottom framed); here $\omega(t) = \mathbf{e}_1 = \text{const}$.

After moving the tool, the null set of $G(\mathbf{x}, t) := F(E^{-1}(t)\mathbf{x})$ represents the tool in the new position, so the motion of the tool generates an envelope Ω given by the points $\mathbf{x}$ where

$$G(\mathbf{x}, t) = \partial_t G(\mathbf{x}, t) = 0 \qquad \text{for some } t. \tag{4}$$

We can develop the second term as

$$\partial_t [F(E^{-1}(t)\mathbf{x})] = \nabla F(E^{-1}(t)\mathbf{x}) \cdot \tfrac{d}{dt}E^{-1}(t)\mathbf{x}.$$

If we use the substitution $\mathbf{x} = E\mathbf{y}$, then we get

$$\partial_t [F(E^{-1}(t)\mathbf{x})] = \nabla F(\mathbf{y}) \cdot \left(\tfrac{d}{dt}E^{-1}\right)E\mathbf{y}.$$

Since $(\tfrac{d}{dt}E^{-1})E = -R^T \tfrac{d}{dt}E$, then we can write Eq. (4) as

$$F(\mathbf{y}) = R\nabla F(\mathbf{y}) \cdot \tfrac{d}{dt}E\mathbf{y} = 0. \tag{5}$$

Since the vector $R\nabla F(\mathbf{y})$ is normal to the tool, then the envelope is the set of points that move tangentially to the tool.

To solve Eq. (5) we use a classical geometric argument; see Fig. 8. Fix some height h and draw the circle C_h over the tool, that is,

$$C_h := \{(r(h)\mathbf{n}, h) : (n_1, n_2) \in S^1\}.$$

Consider a sphere S_h with center at the tool axis and touching the tool tangentially at C_h. The center of S_h is

$$\mathbf{p} := (h + rr')\mathbf{e}_3; \tag{6}$$

$$r' = \tan\alpha$$
$$\tan\beta = \tan(\pi/2 - \alpha) = \cot\alpha$$
$$x = r/\tan\beta = r'r$$
$$\|\mathbf{p}\| = h + r'r$$
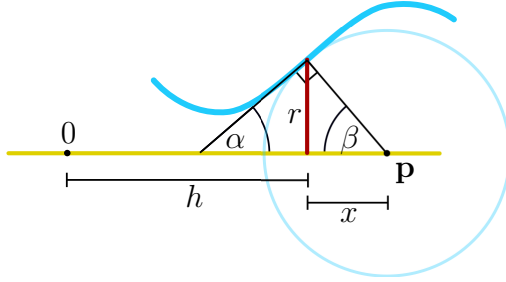
Figure 7: Correspondence between the radial function r and the center $\mathbf{p}$ of the inscribed sphere; see Eq. (6).

When the tool moves, S_h is mapped to ES_h and the velocity of its center $E\mathbf{p}$ is

$$\tfrac{d}{dt}E\mathbf{p} = (h + rr')R\omega \times R\mathbf{e}_3 + \tfrac{d}{dt}\mathbf{a}.$$

Since the great circle $EC'_h := ES_h \cap \{E\mathbf{p} + \mathbf{u} : \mathbf{u} \perp \tfrac{d}{dt}E\mathbf{p}\}$ moves tangentially to ES_h, then any point of the intersection $\mathbf{x}_0 = E\mathbf{y}_0$ between EC_h and EC'_h must satisfy Eq. (5).

It is easier to find $\mathbf{y}_0$ and then to apply E, so we undo the motion E and consider the intersection of the circle C_h with the great circle

$$C'_h = S_h \cap \{\mathbf{p} + \mathbf{u} : \mathbf{u} \perp \mathbf{v}\}, \quad \text{where } \mathbf{v} := R^T\tfrac{d}{dt}E\mathbf{p} = (h + rr')\omega \times \mathbf{e}_3 + R^T\tfrac{d}{dt}\mathbf{a}; \tag{7}$$

the vector $\mathbf{v}$ is the velocity $\tfrac{d}{dt}E\mathbf{p}$ when written in the basis $\{R\mathbf{e}_1, R\mathbf{e}_2, R\mathbf{e}_3\}$. If $\mathbf{y}_0 = (r\mathbf{n}_0, h)$ is the point of the intersection, then $((r\mathbf{n}_0, h) - \mathbf{p}) \cdot \mathbf{v} = 0$, so, after some manipulation, one obtains

$$\mathbf{n}_0 \cdot (v_1, v_2) = r'v_3, \quad \text{with } \mathbf{n}_0 \text{ being a unit vector.} \tag{8}$$

A solution of Eq. (8) has the following form

$$\mathbf{n}_\pm = \frac{r'v_3}{|(v_1, v_2)|}\frac{(v_1, v_2)}{|(v_1, v_2)|} \pm \frac{(-v_2, v_1)}{|(v_1, v_2)|}\sqrt{1 - \left(\frac{r'v_3}{|(v_1, v_2)|}\right)^2}. \tag{9}$$

In general, depending on the sign of the square root in Eq. (9), one gets no or two real solutions. However, there exist two singular cases: one solution and infinitely many. One
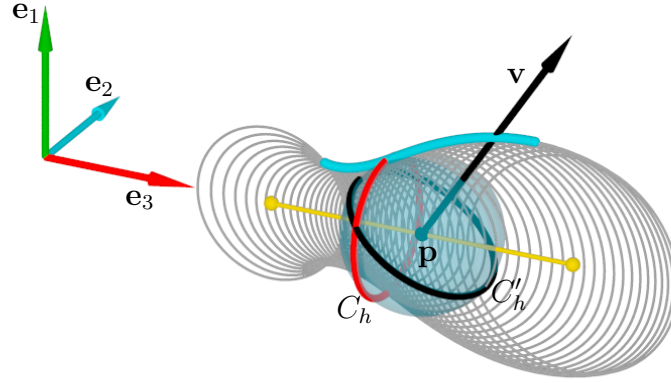
9

Figure 8: The tool is considered as a one parameter family of spheres centered along the finite axis (yellow) with the direction of the $\mathbf{e}_3$ vector. The intersection of the tool with the $x_1 = 0$ plane gives a one-parameter family of circles (gray) and the meridian curve (blue). For a given point $\mathbf{p}$ on the axis, the inscribed sphere S_h (transparent) touches the tool along a circle C_h (red). The instantaneous velocity vector $\mathbf{v}$ defines a great circle C'_h (black) on S_h and its intersection with C_h gives the point(s) of the characteristic. Depending on $\mathbf{v}$, there can be 0, 1, or 2 solutions (intersection of two circles on a single sphere).

solution appears when the square root is equal to zero. Infinitely many solutions occur when $r' = 0$ — it corresponds to the extreme points on the meridian with respect to the distance from the axis. Then the contact circle (red in Fig. 8) becomes a great circle on S_h, and it can coincide with C'_h if and only if $\mathbf{v}$ is parallel to the tool axis vector. In such a case, one obtains infinitely many solutions.

A natural parameterization of the envelope is given by $\psi : (t, h) \mapsto E(r\mathbf{n}_\pm, h)$. We denote the two branches of the envelopes as $\Omega_\pm$. As we are interested in the machining application, only the branch of the envelope closer to the reference surface is relevant. Therefore, from now on, unless stated differently, we consider only that branch and use the notation Ω for it.

3 C^1 Continuity: Proof of Theorem A

This section is dedicated to Theorem A. In Section 3.1 we state precisely the Theorem, and motivate it with an example. In Section 3.2 we prove technical lemmas about envelopes in which we relate properties of the implicit description of the envelope using G with properties of its parameterization ψ. In Section 3.3 we extend the Inverse Function Theorem to a setting where the function is not C^1 everywhere; as it is clear from Theorem 3, if G is only C^1, then the classical Implicit Function Theorem does not work because we need two derivatives for G. Finally, in Section 3.4 we prove that the envelope is C^1 by showing that it is the graph of a smooth function.

3.1 Statement of the Theorem and motivation

Theorem 4. *Suppose that the tool radius function r and the motion E are both piece-wise C^2 but globally only C^1, that the right and left limits of the second derivatives always exist and are finite, that Eq. (8) always has exactly two solutions, and that $\partial_t^2 G = \partial_t^2[F(E^{-1}\mathbf{x})]$ satisfies $|\partial_t^2 G| \geq c > 0$ and it always has the same sign wherever it is defined. Then, the envelope Ω is locally C^1.*

As we mentioned in the Introduction, by *locally C^1* we mean that for a small time interval, and a segment of the tool, the envelope is a usual C^1-surface. However, if we do not impose any restriction on the trajectory or the tool, then the envelope may not be *globally C^1* because of possible self-intersections. Theorem 4 does not give any criteria about how large the time interval or segment of the tool should be to avoid self-intersections, so it does not address the problem of possible global self-intersections.

As we saw in Theorem 3, the envelope is C^1 on the patches where the functions are C^2, so the objective is to find a re-parameterization around every point so that the surface is C^1 locally; see Fig. 9.

Since the first derivatives are continuous, then the vectors $R\nabla F$ are always well-defined, continuous, and perpendicular to the tool. The core of the proof will be to rule out any possible 180°-folding along the edges where the functions lose the second derivative. It is important to notice that $\nabla\psi$ is well-defined only at the points (t, h) where the functions are C^2.

Before starting the proof of Theorem 4, we illustrate it with an example.

Example 3. *Suppose that the tool and the motion are designed using quadratic B-splines with a single knot; see Fig. 9 and also the attached video. Hence, the tool is C^2 except at a point $h_0 = 0$ (red circle in Fig. 9), and the motion is C^2 except at a single time $t_0 = 1$, where $t \in [0, 2]$, so the natural parameterization of the envelope $\psi : (t, h) \mapsto E(r\mathbf{n}, h) + \mathbf{a}$ is not C^1 over the red curves.*

Since the envelope is C^∞ outside the red curves, then at $\psi(t_0, h_0) = \psi(1, 0)$ the envelope is locally a union of four different quadratic surfaces preserving tangency across the red curves; as a 1D analogue, the reader can think of the C^1 function $x|x|$ at $x_0 = 0$. Even though neither the characteristic curves nor the stream curves are C^1 when they cross the red curves, the envelope is still C^1.

3.2 Technical lemmas about envelopes

We need to relate some properties of G with those of the parameterization ψ. The main result of this subsection, Lemma 6, shows that as long as we are away from the edge of regression, that is, $\partial_t^2 G$ does not change sign, then the normal vector of the envelope does not change direction abruptly. In Example 2 the reader can see the sudden change of direction at the cusp.

To ensure that the characteristic curves are well-defined for envelopes in general, we need to assume that $\nabla_\mathbf{x} G \times \nabla_\mathbf{x} \partial_t G \neq 0$. However, notice that we have said nothing about this
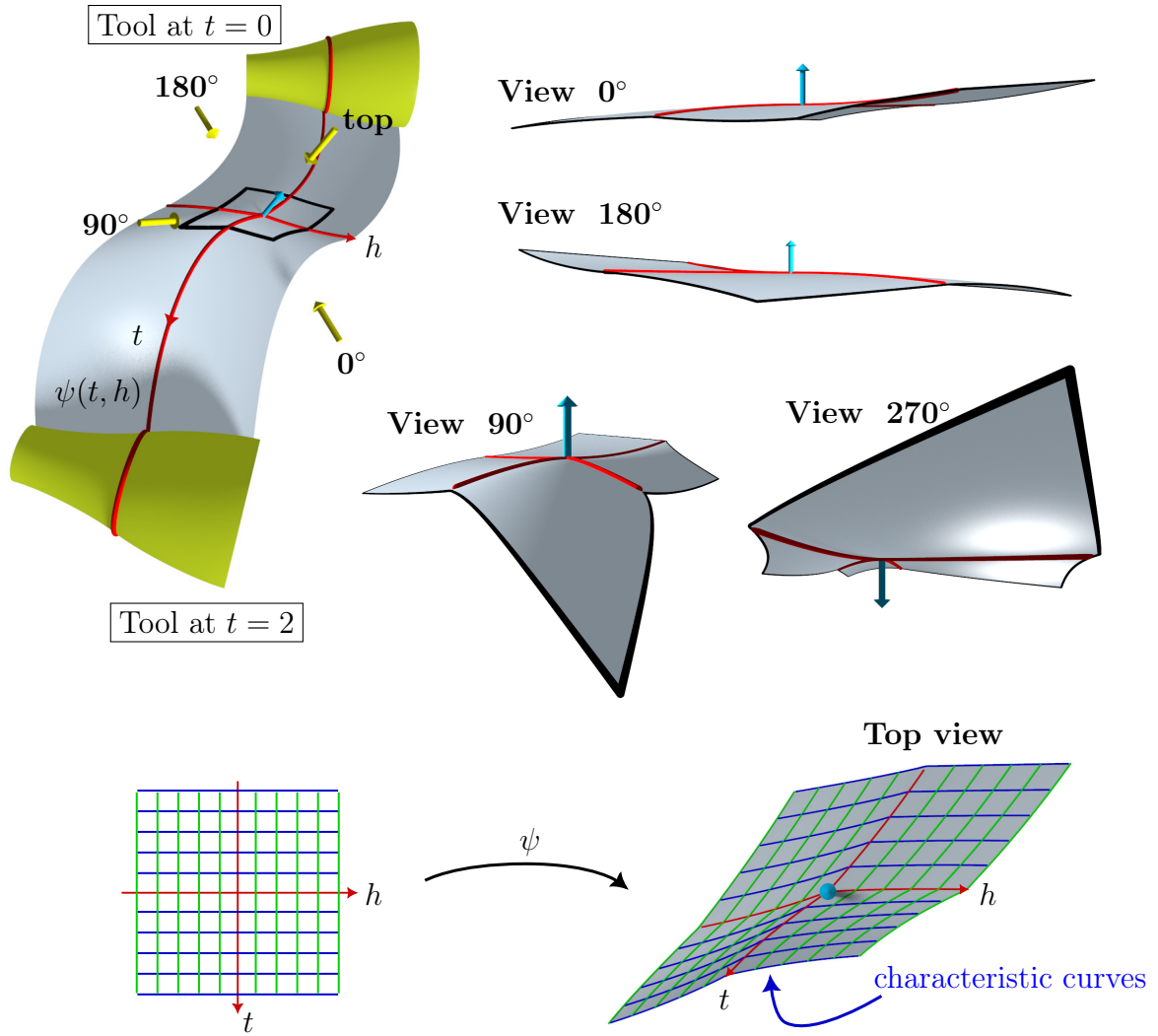
Figure 9: Top left: The tool is not C^2 over the red circle, and the red curves on the envelope are the points where the natural parameterization is not C^1. The blue arrow at $\psi(t_0, h_0)$ represents the normal vector. The yellow arrows indicate different viewpoints, four of them from points on the tangent plane (one arrow is hidden behind the envelope). Top right: At $0°$ or $180°$ the envelope is evidently flat. At $90°$ or $270°$ (in this view we flipped the normal vector) we see how the envelope bends at $\psi(t_0, h_0)$, which makes the normal vector looks slanted in the left image. Bottom: The blue lines are the characteristic curves $h \mapsto \psi(t, h)$, and the green lines are the stream curves $t \mapsto \psi(t, h)$.

12

in the statement of Theorem 4; instead, we have assumed that Eq. (8) has two solutions. In the following lemma, we will show that the existence of characteristic curves implies that the cross product does not vanish.

Lemma 5. *Suppose that r and E are both C^2 continuous, and that Eq. (8) has exactly two different solutions. Then,*

$$\partial_h \psi = \pm |\partial_h \psi| \frac{\nabla_{\mathbf{x}} G \times \nabla_{\mathbf{x}} \partial_t G}{|\nabla_{\mathbf{x}} G \times \nabla_{\mathbf{x}} \partial_t G|}, \tag{10}$$

where the sign $\pm$ is the same as in Eq. (9).

Proof. We already know that $\nabla_{\mathbf{x}} G = R \nabla F$, so we have to compute $\nabla_{\mathbf{x}} \partial_t G$:

$$\nabla_{\mathbf{x}} \partial_t G = (\tfrac{d}{dt} R) \nabla F(\mathbf{y}) - R D^2 F(\mathbf{y}) R^{-1} \tfrac{d}{dt} E \mathbf{y}.$$

Since $\nabla F(\mathbf{y}) = (-y_1, -y_2, rr')$, then by re-ordering terms we have

$$\nabla_{\mathbf{x}} \partial_t G = (\tfrac{d}{dt} R)[-\mathbf{y} + (y_3 + rr') \mathbf{e}_3] + \tfrac{d}{dt} E \mathbf{y} - (1 + (r')^2 + rr'')(\tfrac{d}{dt} E \mathbf{y} \cdot R \mathbf{e}_3) R \mathbf{e}_3$$
$$= (y_3 + rr') \tfrac{d}{dt} R \mathbf{e}_3 + \tfrac{d}{dt} \mathbf{a} + (\cdots) R \mathbf{e}_3.$$

We put the term involving r'' under the hood in $(\cdots)$ because it will not play any important role. Recalling the definition of $\mathbf{v}$ in Eq. (7), we have

$$\nabla_{\mathbf{x}} \partial_t G = R(\mathbf{v} + (\cdots) \mathbf{e}_3).$$

Taking cross product with $\nabla_{\mathbf{x}} G = R \nabla F = -(y_1, y_2, 0) + rr' \mathbf{e}_3$ we have

$$\nabla_{\mathbf{x}} G \times \nabla_{\mathbf{x}} \partial_t G = R[(-(y_1, y_2, 0) + rr' \mathbf{e}_3) \times ((v_1, v_2, 0) + ((\cdots) + v_3) \mathbf{e}_3)]$$
$$= R[-(y_1, y_2, 0) \times (v_1, v_2, 0) + \mathfrak{R}].$$

The residue $\mathfrak{R}$ is a vector orthogonal to $\mathbf{e}_3$, so it does not interfere with the first term.

If we take $\mathbf{y} = (r \mathbf{n}_\pm, h)$ in the characteristic curve, then from Eq. (9) we get

$$-(y_1, y_2, 0) \times (v_1, v_2, 0) = \pm r |(v_1, v_2)| \left[1 - \left(\frac{r' v_3}{|(v_1, v_2)|}\right)^2\right]^{1/2} \mathbf{e}_3 := \pm q \, \mathbf{e}_3,$$

where $q > 0$ if there are exactly two solutions $\mathbf{n}_\pm$, and we conclude that $\nabla_{\mathbf{x}} G \times \nabla_{\mathbf{x}} \partial_t G \neq 0$.

Recall that $\psi(t, h) = E(r\mathbf{n}, h)$, so $\partial_h \psi = R(\partial_h (r\mathbf{n}), 1)$. Since $\partial_h \psi$ and $\nabla_{\mathbf{x}} G \times \nabla_{\mathbf{x}} \partial_t G$ are proportional, then Eq. (10) necessarily holds. $\qquad\square$

It is worth noticing that Lemma 5 implies that the property $\nabla_{\mathbf{x}} G \times \nabla_{\mathbf{x}} \partial_t G \neq 0$ is stable under perturbations with small derivative. More explicitly, if E is perturbed as $\tilde{E} := E + \delta E$, where $\sup_t \|\tfrac{d}{dt} \delta E\|$ is sufficiently small, then $\nabla_{\mathbf{x}} \tilde{G} \times \nabla_{\mathbf{x}} \partial_t \tilde{G} \neq 0$ even though this expression involves second derivatives, which are not under control. Unfortunately, the property $\partial_t^2 G \neq 0$ is not that stable.

The significance of this stability property is that, for example, if one plans a tool motion with $\nabla_{\mathbf{x}} G \times \nabla_{\mathbf{x}} \partial_t G \neq 0$ for all time, then this property will be preserved if one controls well the velocity (first derivative), no matter how large the acceleration (second derivative) is. However, if we control the velocity but not the acceleration, then the envelope can lose smoothness because $\partial_t^2 \tilde{G} = 0$ could happen; see Example 4.
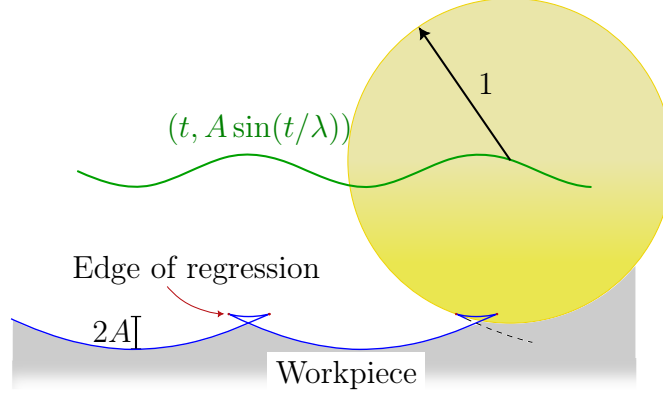
Figure 10: A 2D example. The center of a disk of radius 1 moves as $\mathbf{a}(t) = (t, A\sin(t/\lambda))$; here, $A = 0.1$ and $\lambda = 0.224$, but A can be taken arbitrarily small. Even though the motion is smooth, and the velocity departs slightly from a straight line if $A \ll \lambda$, the envelope (blue) contains cusps if $A > \lambda^2$, which results in a scalloped surface finish.

Example 4. *Let us consider a disk of radius 1 moving in 2D; see Fig. 10. Even though the motion of the center of the disk is smooth (and infinitely differentiable), and arbitrarily close to a straight line, $\partial_t^2 G$ changes signs which causes cusps on the envelope of the disk. This 2D example can be directly brought to 3D by extruding the whole scene in a direction perpendicular to the plane, and the negative impact on the machining application is clear as the workpiece would become only C^0 continuous.*

Lemma 6. *If $\psi : (t, h) \mapsto E(r\mathbf{n}_\pm, h)$, where $\mathbf{n}_\pm$ is given by Eq. (9), then*

$$\partial_t \psi \times \partial_h \psi = \mp \frac{|\partial_h \psi| \partial_t^2 G}{|\nabla_\mathbf{x} G \times \nabla_\mathbf{x} \partial_t G|} \nabla_\mathbf{x} G, \quad \text{whenever it is defined,}$$

where $\pm$ refers to the sign in the subscript of $\mathbf{n}_\pm$.

Not surprisingly, $\partial_t \psi \times \partial_h \psi$ is parallel to $\nabla_x G = R\nabla F$. The important conclusion is that the sign of $\partial_t^2 G$ determines whether the cross product points in the same direction of $R\nabla F$ or not for each envelope $\Omega_\pm$.

Proof. By differentiating $\partial_t G(\psi(t, h), t) = 0$ with respect to t we get

$$\partial_t^2 G = -\nabla_\mathbf{x} \partial_t G \cdot \partial_t \psi.$$

Let us choose the basis vectors

$$\mathbf{k_1} := \nabla_\mathbf{x} G = R\nabla F, \quad \mathbf{k_2} := \nabla_\mathbf{x} \partial_t G, \quad \text{and} \quad \mathbf{k_3} := \frac{\mathbf{k_1} \times \mathbf{k_2}}{|\mathbf{k_1} \times \mathbf{k_2}|}.$$

We denote the dual basis as $\mathbf{k}' = \{\mathbf{k_1'}, \mathbf{k_2'}, \mathbf{k_3'}\}$, so it satisfies $\mathbf{k_i'} \cdot \mathbf{k_j} = \delta_{ij}$; in particular, $\mathbf{k_3'} = \mathbf{k_3}$. Since $\nabla_\mathbf{u} \psi$ is orthogonal to $\mathbf{k_1}$ for every $\mathbf{u} = (u_1, u_2)$, and $\partial_h \psi$ is tangent to the characteristic curve, then

$$\partial_t \psi = -\partial_t^2 G \, \mathbf{k_2'} + a\mathbf{k_3'} \quad \text{and} \quad \partial_h \psi = \pm|\partial_h \psi|\mathbf{k_3'};$$

14

the last identity corresponds to Lemma 5. Then, using a cross product yields the important identity

$$\partial_t \psi \times \partial_h \psi = \mp |\partial_h \psi| \partial_t^2 G \, \mathbf{k}_2' \times \mathbf{k}_3' = \mp \frac{|\partial_h \psi| \partial_t^2 G}{|\nabla_\mathbf{x} G \times \nabla_x \partial_t G|} \nabla_\mathbf{x} G.$$

$\square$

3.3   A generalization of the Inverse Function Theorem

To prove that a re-parameterization exists, we will need a generalization of the Inverse Function Theorem, but let us introduce one definition first.

Definition 7. *An m-polygonal mesh in $\mathbb{R}^2$ is a graph where the edges are straight lines, and each vertex has valence $\leq m$. We say that the mesh is convex if every polygon is convex.*

The following is a generalization of the Inverse Function Theorem in $\mathbb{R}^2$.

Lemma 8. *Suppose that $\varphi : U \subset \mathbb{R}^2 \to \mathbb{R}^2$ is C^1 continuous except at most in a convex 4-polygonal mesh, that $D\varphi$ can be extended continuously up to the boundary in every polygonal patch, and that $\det D\varphi$ satisfies $|\det D\varphi| \geq c > 0$, and it never changes the sign wherever it is defined. Then, φ is a local homeomorphism.*

In Lemma 8, the extensions of $D\varphi$ up to the boundary do not have to agree over the edges; otherwise, φ would be C^1 continuous everywhere.

Suppose that the tool and the motion are not C^2 continuous at heights $h_1, \ldots, h_N$ and times $t_1, \ldots, t_M$, respectively. We will apply Lemma 8 to the mesh generated by the lines $t \mapsto (t, h_i)$, for $i = 1, \ldots, N$, and $h \mapsto (t_j, h)$, for $j = 1, \ldots, M$. Recall Fig. 9 and the red lines in the (t, h)-plane forming a mesh.

Interestingly enough, Lemma 8 is false for m-polygonal meshes with $m \geq 5$; the proof goes beyond the scope of the paper. Moreover, the discretization of envelopes are naturally regular quad meshes, so in our case $m = 4$ everywhere.

Proof. For definiteness, we assume that $\det D\varphi \geq c > 0$ everywhere. Since the conclusions are local, we will always assume that U is a ball $B(0, r)$ with $r \ll 1$, and that $\varphi(0) = 0$. In the open patches φ is a C^1 continuous function, so we can apply the classical Inverse Function Theorem. Therefore, we will assume that 0 is a vertex of the mesh where the edges $E_1, \ldots, E_4$ (ordered counter-clockwise) meet; see Fig. 11. We denote by P_i the *open* patch between E_i and E_{i+1}; and by the assumptions on regularity, $E_5 = E_1$. Also, we refer to φ over the patch P_i as φ^i.

Our first task will be to see that φ is injective. In the closure of each patch φ is injective because $D\varphi$ is continuous and invertible, so we only need to rule out any possible folding of one patch over the other.

Let $\bar{\mathbf{e}}_i$ be the unit vector pointing in the direction of the edge E_i.[2] By continuity $\varphi^{i-1}(s\bar{\mathbf{e}}_i) = \varphi^i(s\bar{\mathbf{e}}_i)$, so taking $s \to 0^+$ we see that $D\varphi^{i-1}(0)(\bar{\mathbf{e}}_i) = D\varphi^i(0)(\bar{\mathbf{e}}_i)$. Shrinking U if necessary, we can assume that the curves $\varphi(E_i)$ (the images of $s \mapsto \varphi(s\bar{\mathbf{e}}_i)$) remain close to the straight lines $s \mapsto sD\varphi^i(0)(\bar{\mathbf{e}}_i)$.

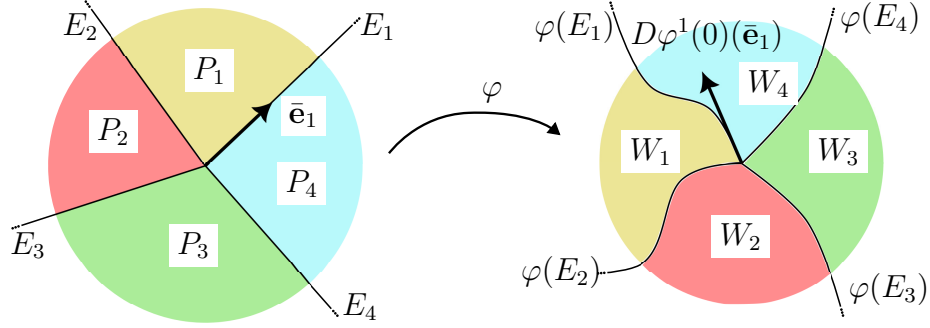[2]$\bar{\mathbf{e}}_i$ should not be confused with the vectors of the canonical basis $\mathbf{e}_i$.

Figure 11: The function φ maps the patches $P_1, \ldots, P_4$ counter-clockwise, and they only turn once around the origin.

By the definition of the Jacobian

$$\det D\varphi(0) = \frac{\sin\Theta |D\varphi^i(0)(\bar{\mathbf{e}}_i)||D\varphi^i(0)(\bar{\mathbf{e}}_{i+1})|}{\sin\theta},$$

where θ is the angle between $\bar{\mathbf{e}}_i$ and $\bar{\mathbf{e}}_{i+1}$, and Θ the angle between $D\varphi^i(0)(\bar{\mathbf{e}}_i)$ and $D\varphi^i(0)(\bar{\mathbf{e}}_{i+1})$. Since the mesh is convex, $\sin\theta > 0$, and the condition $\det D\varphi(0) > 0$ forces $D\varphi^i(0)(\bar{\mathbf{e}}_{i+1})$ to lie at an angle $< \pi$ of $D\varphi^i(0)(\bar{\mathbf{e}}_i)$ counter-clockwise; see Fig. 11.

We will show that $\varphi(P_i)$ stays in the open set W_i between $\varphi(E_i)$ and $\varphi(E_{i+1})$. Suppose on the contrary that for some $\mathbf{p}$ in P_i its image $\varphi(\mathbf{p})$ lies outside W_i. Then we join $\mathbf{p}$ and a point $\mathbf{q} = \rho\bar{\mathbf{e}}_i$ with the line $\alpha : s \mapsto (1-s)\mathbf{q} + \mathbf{p}s \in P_i$ and define

$$s_0 = \sup\{0 < s \le 1 : \varphi(\alpha(s)) \in W_i\}.$$

Since $\det D\varphi > 0$ then $\varphi \circ \alpha(s)$ enters W_i when s is small, which implies $s_0 > 0$. Since $\varphi \circ \alpha(1) \notin W_i$ then $\varphi \circ \alpha(s_0) \in \varphi(E_i) \cup \varphi(E_{i+1})$. However, $\alpha(s_0) \notin E_i \cup E_{i+1}$, which contradicts the injectivity of φ in the closure of P_i.
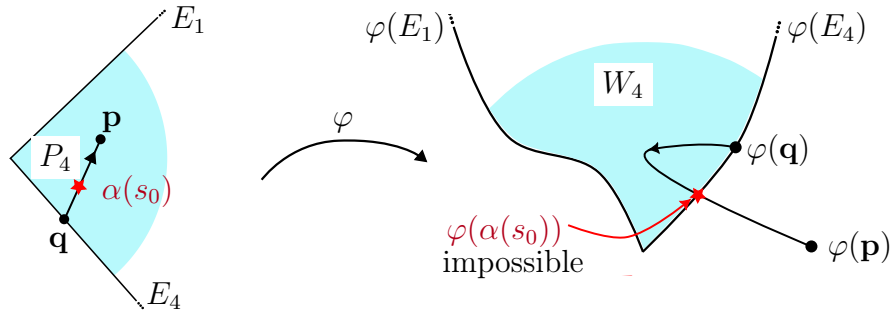

Figure 12: $\varphi(P_4)$ cannot escape from the region in between the lines $\varphi(E_1)$ and $\varphi(E_4)$.

We know that $P_1, \ldots, P_4$ are mapped counter-clockwise inside the sets $W_1, \ldots, W_4$, so two consecutive patches cannot fold one over the other, but it is still possible that $W_1 \cup \cdots \cup W_4$ covers the plane more than once; we show that this is not the case. In fact, the angle between

16

$D\varphi^i(\bar{\mathbf{e}}_i)$ and $D\varphi^i(\bar{\mathbf{e}}_{i+1})$ is $< \pi$, so the total angle spanned from $D\varphi^1(\bar{\mathbf{e}}_1)$ going back to itself $(= D\varphi^5(\bar{\mathbf{e}}_5))$ is $< 4\pi$, but the angle must be a multiple of 2π, so it has to be 2π. Hence, the union $W_1 \cup \cdots \cup W_4$ covers the plane only once, which in turn implies that φ is injective in U.

It remains to prove that the inverse φ^{-1} is continuous. For this, it suffices to show that for any sufficiently small ball $B(\mathbf{p}, \rho) \subset U$, its image $\varphi(B(\mathbf{p}, \rho))$ contains a ball. Again, the only interesting case is the vertex $\mathbf{p} = 0$. However, we have shown that φ winds once around 0, so the *winding number* of $\varphi(\rho S^1)$ around 0 does not vanish. This implies that there exists a ball D around 0 such that for every $\mathbf{w} \in D$ the equation $\varphi(\mathbf{u}) = \mathbf{w}$ has a solution $\mathbf{u} \in B(0, \rho)$; see [2, Section 8] for a thorough discussion about the winding number. This concludes the proof of Lemma 8. $\qquad\square$

3.4 The envelope as the graph of a function C^1

We are almost done with the proof of Theorem 4, and we will show that the envelope can be seen as the graph of a smooth function in small neighborhoods.

For any point $\mathbf{p} \in \Omega$ we have the parameterization $\psi : (t, h) \mapsto E(r\mathbf{n}, h)$. After some transformations, we may assume that $0 \in \Omega$, $\psi(0) = 0$, and $R\nabla F(0) = \lambda \mathbf{e}_3$ for some $\lambda > 0$. We restrict ourselves to a small neighborhood U of 0 where $R\nabla F$ stays close to $R\nabla F(0)$.

Locally, in a sufficiently small neighborhood of the point of interest, one can assume that the envelope is the graph of a function f; that is, f is the Monge's representation of the envelope. Define $\varphi(t, h) = (\psi_1, \psi_2)(t, h)$, which satisfies the conditions of Lemma 8, where the mesh is formed by the lines in the (t, h)-plane where the tool or the motion are not C^2 continuous. We only check here that $\det D\varphi$ has the same sign everywhere in U. In fact,

$$\det D\varphi = (\partial_t \psi \times \partial_h \psi) \cdot \mathbf{e}_3$$
$$= a\, R\nabla F \cdot \mathbf{e}_3,$$

where a does not change sign by Lemma 6 and the assumption about $\partial_t^2 G$ in Theorem 4. Since $R\nabla F \cdot \mathbf{e}_3 > 0$ in U, we can apply Lemma 8 and conclude that φ is a local homeomorphism in U, shrinking it if necessary.

The function $f := \psi_3 \circ \varphi^{-1}$ is the sought after function whose graph is the envelope. The next lemma completes the proof of Theorem 4.

Lemma 9. *Suppose that $f : U \subset \mathbb{R}^2 \to \mathbb{R}$ is C^1 continuous except at most in a set S which is the union of a finite number of segments of C^1 continuous curves, that the normal vector can be extended continuously up to the boundary in every component outside S, and that the extended normal vector is continuous in U. Then, f is C^1 continuous everywhere.*

Proof. For every $\mathbf{p} \in U$ we will prove that f is C^1 continuous in a ball $B := B(\mathbf{p}, r)$, for $r \ll 1$. After a linear transformation if necessary, we can assume that all lines parallel to the coordinate axes intersect $S \cap B$ at most in a finite number of points. To prove Lemma 9, we only need to prove that the partial derivatives exist and are continuous.

Let $\mathbf{N} = (N_1, N_2, N_3)$ denote the normal vector, so $\nabla f = -(N_1/N_3, N_2/N_3)$ wherever ∇f is defined. That is, $N_3 \neq 0$, which is in accordance with our assumption that f is a Monge's parameterization of the envelope. By assumption, we can extend ∇f to a continuous vector field $\tilde{\nabla} f = -(N_1/N_3, N_2/N_3)$ over all U. The function $h(t) = f(z_1 + t, z_2)$, for $z \in B$, is differentiable and $h'(t) = \partial_1 f(z_1 + t, z_2)$, except at most in a finite number of points, but by the mean value theorem h is C^1 continuous everywhere and $h'(t) = \tilde{\partial}_1 f(z_1 + t, z_2)$. The same being true for $\partial_2 f$, we conclude that $f \in C^1(B)$.

$\square$

4 $\quad C^0$ Continuity: Proof of Theorem B

This Section is dedicated to Theorem B. In Section 4.1 we state and prove the Theorem. We complement the formal proof with a graphical description of it. In Section 4.2 we describe the conditions for the continuity of the envelope in a more compact way, and we show a simple construction of C^0 envelopes using this description. Also, paths with both branches of the envelope continuous are described. Finally, in Section 4.3 we include examples showing the relevance of the Main Theorem for machining.

4.1 Main Theorem

Theorem 10. *Suppose that the tool with the radius function r is C^1 continuous, except at a single height h_0, and that the right and left limits of r' at h_0 exist. Then, for every t there are three degrees of freedom available to choose the motion $E \in C^1$ so that Eq. (8) has two solutions and at least one characteristic curve is continuous.*

Proof. We fix a time $t = 0$, and assume that $E(0) = I$.

We denote by S_+ and S_- the two inscribed spheres of the tool centered at $l_+\mathbf{e}_3$ and $l_-\mathbf{e}_3$, intersecting in the circle at height h_0 where the tool is G^0-continuous; see Fig. 13(a).

From Eq. (6) we know that $l_\pm = h_0 + rr'(h_0^\pm)$; the spheres are different because $r'(h_0^-) \neq r'(h_0^+)$. As we did in Section 2, let $\mathbf{v}_+$ and $\mathbf{v}_-$ denote the velocity at the center of the spheres S_+ and S_-, respectively. Recall from Eq. (7) that

$$\mathbf{v}_\pm = l_\pm \tfrac{d}{dt} R\mathbf{e}_3(0) + \tfrac{d}{dt}\mathbf{a}(0).$$

Notice that $\tfrac{d}{dt} R(0)\mathbf{e}_3$ is orthogonal to $\mathbf{e}_3$, so

$$v_{+,3} = v_{-,3} = \tfrac{d}{dt} a_3(0).$$

We can re-parameterize the motion so that $|\mathbf{v}_+| = 1$.

If $\mathbf{x}_\pm$ are the limits of a characteristic curve at h_0 from above and below, then Theorem 10 asserts that we can find a motion, represented by $\mathbf{v}_+$ and $\mathbf{v}_-$, such that $\mathbf{x}_+ = \mathbf{x}_- = \mathbf{x}_0$. From Eq. (8) we see that

$$\mathbf{v}_+ \cdot \mathbf{x}_0 = l_+ \tfrac{d}{dt} a_3(0) \quad \text{and} \quad \mathbf{v}_- \cdot \mathbf{x}_0 = l_- \tfrac{d}{dt} a_3(0). \tag{11}$$
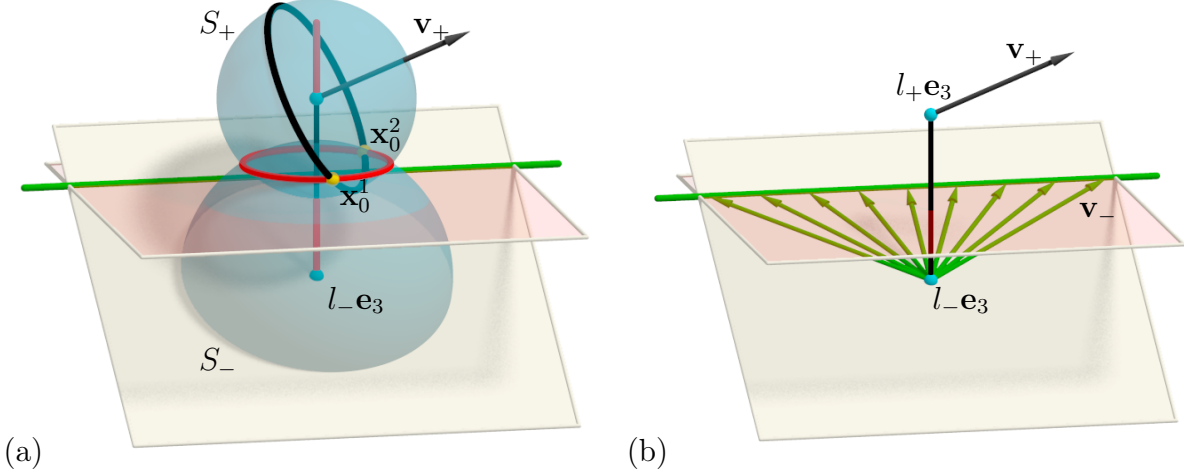
Figure 13: G^0-ness of an envelope controlled by an instantaneous motion. (a) The two limit spheres S_+ and S_- of the meridian point with only G^0 continuity intersect at a circle (red). The instantaneous velocity vector at the center of S_+, $\mathbf{v}_+$, defines a great circle on S_+ (black), which intersected with the red circle yields two points $\mathbf{x}_0^1$ and $\mathbf{x}_0^2$ of the characteristic at height h_0. To be C^0 continuous, the characteristic must pass through $\mathbf{x}_0^1$, which forms a linear constraint Eq. (13) on $\mathbf{v}_-$ (light plane). The other linear constraint is the rigidity of the axis (red transparent plane). (b) The two planes generically intersect at a line (green), which is a locus of endpoints of $\mathbf{v}_-$ such that the tool is rigid and the envelope G^0.

The first equation has two solutions $\mathbf{x}_0^1$ and $\mathbf{x}_0^2$ if and only if

$$|r'(h_0^+)\tfrac{d}{dt}a_3(0)| < \sqrt{v_{+,1}^2 + v_{+,2}^2};$$

see for example Eq. (9). Since $|\mathbf{v}_+| = 1$ and $v_{+,3} = \frac{d}{dt}a_3(0)$, then we can re-write the above condition as

$$|v_{+,3}| < \frac{1}{\sqrt{1 + |r'(h_0^+)|^2}}. \tag{12}$$

Hence, with the normalization condition $|\mathbf{v}_+| = 1$, one has *two degrees of freedom* to choose the initial velocity vector on the unit sphere, i.e., $\mathbf{v}_+ \in V \subset S^2$, where V is the open set where Eq. (12) holds. Once we fix $\mathbf{v}_+$, we can choose one solution $\mathbf{x}_0$, and then we have *one degree of freedom* to choose $\mathbf{v}_-$ from the straight line solving the second equation in Eq. (11); three degrees of freedom in total. $\qquad \square$

A geometric reasoning of the proof of Theorem 10 is depicted in Fig. 13. Draw the circle C_0 on the tool at height zero, and call $\mathbf{x}_+$ the intersection between C_0 and the great circle

$$C_+' := S_+ \cap \{\mathbf{q} + \mathbf{z} : \mathbf{z} \perp \mathbf{v}_+\}.$$

As we saw in Section 2, $\mathbf{x}_+$ belongs to the characteristic curve, so we have to choose $\mathbf{v}_-$ so that the limits of the characteristic curve $\mathbf{x}_-$ and $\mathbf{x}_+$ coincide.

19

We draw a line L passing through $\mathbf{p} = l_-\mathbf{e}_3$ and $\mathbf{x}_+$. Each plane containing L generates a great circle in S_- that intersects $\mathbf{x}_+$, so $\mathbf{v}_-$ must be perpendicular to L, that is,

$$\mathbf{v}_- \cdot (\mathbf{x}_+ - \mathbf{p}) = 0. \tag{13}$$

Since $v_{-,3} = v_{+,3}$ is known, then we can find the first two components of $\mathbf{v}_-$ by solving Eq. (13). Since $\mathbf{p} = l_-\mathbf{e}_3$, then

$$\mathbf{v}_- \cdot \mathbf{x}_+ = l_-v_{-,3},$$

which corresponds to Eq. (8) with $\mathbf{x}_- = \mathbf{x}_+$. Consequently, one has two degrees of freedom to choose $\mathbf{x}_+$, and one degree of freedom to choose $\mathbf{x}_-$ (green line in Fig. 13), three in total.

4.2 Some consequences of the Main Theorem

Now, we want to find conditions that allow us to decide whether a given motion has a continuous characteristic curve.

Lemma 11. *Let the tool be defined as in Theorem 10, and let $\mathbf{x}_0 = E(t_0)\mathbf{y}_0$ be a point on the tool where it is not C^1 continuous. Then, $\mathbf{x}_0$ belongs to a continuous characteristic curve if and only if*

$$\tfrac{d}{dt}\mathbf{a} \cdot R\mathbf{y}_0 = 0 \qquad and \qquad \tfrac{d}{dt}R\mathbf{e}_3 \cdot R\mathbf{y}_0 = \tfrac{d}{dt}\mathbf{a} \cdot R\mathbf{e}_3. \tag{14}$$

Equivalently, if and only if

$$(\tfrac{d}{dt}E)\mathbf{y}_0 \cdot R\mathbf{y}_0 = 0. \qquad and \qquad (\tfrac{d}{dt}E)\mathbf{y}_0 \cdot R\mathbf{e}_3 = 0. \tag{15}$$

Proof. We assume that $t_0 = 0$. Without loss of generality, we again assume that $E(0) = I$ so that $\mathbf{x}_0 = \mathbf{y}_0$.

We expand Eq. (11) as

$$(l_+\tfrac{d}{dt}R\mathbf{e}_3 + \tfrac{d}{dt}\mathbf{a}) \cdot \mathbf{x}_0 = l_+\tfrac{d}{dt}a_3$$
$$(l_-\tfrac{d}{dt}R\mathbf{e}_3 + \tfrac{d}{dt}\mathbf{a}) \cdot \mathbf{x}_0 = l_-\tfrac{d}{dt}a_3.$$

From these equations and some algebraic manipulation we get

$$\tfrac{d}{dt}\mathbf{a} \cdot \mathbf{y}_0 = 0 \qquad and \qquad \tfrac{d}{dt}R\mathbf{e}_3 \cdot \mathbf{y}_0 = \tfrac{d}{dt}a_3,$$

which is Eq. (14) with $R = I$ being the identity. For a general motion E, we apply the previous result to $E_m = E^{-1}(0)E$, and we use the relationships $R_m = R^T(0)R$ and $\mathbf{a}_m = R^T(0)(\mathbf{a} - \mathbf{a}(0))$.

The first equation in Eq. (15) is

$$(\tfrac{d}{dt}E)\mathbf{y}_0 \cdot R\mathbf{y}_0 = \tfrac{d}{dt}R\mathbf{y}_0 \cdot R\mathbf{y}_0 + \tfrac{d}{dt}\mathbf{a} \cdot R\mathbf{y}_0 = \tfrac{d}{dt}\mathbf{a} \cdot R\mathbf{y}_0 = 0;$$

in the last identity we used the first equation in Eq. (14).

The second equation in Eq. (15) is

$$(\tfrac{d}{dt}E)\mathbf{y}_0 \cdot R\mathbf{e}_3 = \tfrac{d}{dt}R\mathbf{y}_0 \cdot R\mathbf{e}_3 + \tfrac{d}{dt}\mathbf{a} \cdot R\mathbf{e}_3 = -\tfrac{d}{dt}R\mathbf{e}_3 \cdot R\mathbf{y}_0 + \tfrac{d}{dt}\mathbf{a} \cdot R\mathbf{e}_3 = 0;$$

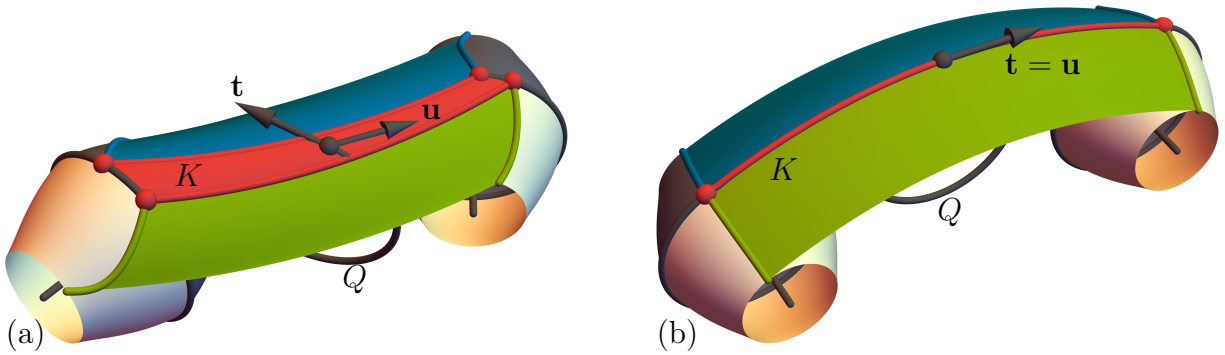again, in the last identity we used the second equation in Eq. (14). $\square$

Figure 14: A tool envelope with a C^1 discontinuity along a circle Q is C^0 continuous if and only if the surface K (generated by sweeping the corresponding part of Q) degenerates into a curve. This happens if and only if the velocity vector $\mathbf{u}$ at any point of Q coincides (up to scaling and orientation) with the tangent vector $\mathbf{t}$ of Q at that point. Left: The envelope contains a gap, so K is not degenerated. Right: The envelope is C^0 continuous and K degenerates into a curve.

Remark 2. Let us look at a discontinuity in the envelopes from a different point of view. Let Q denote a circle along which the tool has a C^1 discontinuity. Then the discontinuity in the envelope can be filled by the surface K generated by the sweep of the corresponding part of the circle Q. The envelope is C^0 if and only if the surface K degenerates into a curve. This happens if and only if the velocity $\mathbf{u}$ at any point of Q is tangent to Q; see Fig. 14. This is exactly what is stated in Eq. (15) of Lemma 11.

We will now use Lemma 11, in particular Eq. (15), to give a simple method for constructing continuous envelopes. Suppose that the tool is C^1-discontinuous at a single point $h_0 = 0$, and let γ be the curve in the envelope traced out by $t \mapsto E(r(h_0)\mathbf{n}, h_0)$. To find E, we assume that we are given the curve γ with $\frac{d}{dt}\gamma \neq 0$ everywhere.

By definition

$$\tfrac{d}{dt}\gamma = \lambda \tfrac{d}{dt}[E(r\mathbf{n}, 0)] = \lambda(\tfrac{d}{dt}E)(r\mathbf{n}, 0) + \lambda R(r\tfrac{d}{dt}\mathbf{n}, 0) \qquad \text{for some } \lambda \neq 0.$$

By Eq. (15) we have to ensure that

$$(\tfrac{d}{dt}\gamma) \cdot R(r\mathbf{n}, 0) = \lambda r^2 \tfrac{d}{dt}\mathbf{n} \cdot \mathbf{n} = 0 \quad \text{and} \quad (\tfrac{d}{dt}\gamma) \cdot R\mathbf{e}_3 = \lambda(r\tfrac{d}{dt}\mathbf{n}, 0) \cdot \mathbf{e}_3 = 0.$$

This tells us that $\{\mathbf{T}, R(r\mathbf{n}, 0), R\mathbf{e}_3\}$ is an orthogonal basis, where $\mathbf{T}$ is the tangent vector of γ. Recall that $R(r\mathbf{n}, 0)$ is perpendicular to the tool, and $R\mathbf{e}_3$ is the tool axis, so in some sense the envelope touches the tool tangentially, despite the lack of the tangent plane at $h_0 = 0$.

If $\gamma \in C^3$, then we can express $R(r\mathbf{n}, 0)$ and $R\mathbf{e}_3$ in terms of the Frenet–Serret frame. Recall that the normal of the curve is $\mathbf{N} := \frac{d}{dt}\mathbf{T}/\kappa$, where κ is the curvature, and the binormal vector is $\mathbf{B} = \mathbf{T} \times \mathbf{N}$.
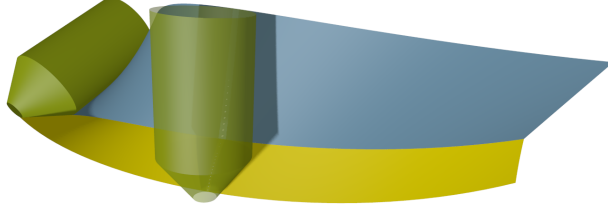
21

Figure 15: A C^0 continuous tool sweeping a continuous envelope. The tool follows the path $\gamma(t) = (-t^2/4, t, t^3/8)$, and the tool is the union of a cylinder of radius 0.2 and length 0.6, and a truncated cone with smaller radius 0.05 and length 0.2.

We have the freedom to choose R as long as the tool axis remains perpendicular to $\mathbf{T}$. The direction of the tool axis is

$$R\mathbf{e}_3 = \sin\theta\,\mathbf{N} + \cos\theta\,\mathbf{B},$$

where $\theta \in C^1$ is a free parameter, and it represents the angle between the osculating plane and the normal plane to $R\mathbf{e}_3$; clearly $\mathbf{T} \cdot R\mathbf{e}_3 = 0$. This is enough information to recover R modulo a rotation around the x_3-axis which does not have any effect. Since $\gamma \in C^3$ then $R \in C^1$.

To find $\mathbf{a}$ we use

$$R(\mathbf{n}, 0) = \cos\theta\,\mathbf{N} - \sin\theta\,\mathbf{B};$$

notice that $\mathbf{T} \cdot R(r\mathbf{n}, 0) = 0$, as it should be. The translation is then recovered as $\mathbf{a} = \gamma - R(r\mathbf{n}, 0) \in C^1$. In Fig. 15 this method was used to construct a continuous envelope.

We can also use Lemma 11 to describe the motions that preserve the continuity of both characteristic curves.

Theorem 12. *Let the tool be defined as in Theorem 10 with a C^1-discontinuity at $h_0 = 0$. Both characteristic curves are continuous if and only if either*

$$(i)\; R\mathbf{e}_3 = \mathbf{T}, \quad or$$
$$(ii)\; R\mathbf{e}_3 = \cos(\textstyle\int \tau + c)\,\mathbf{N} - \sin(\textstyle\int \tau + c)\,\mathbf{B}, \quad where\; c\; is\; a\; constant.$$

Here, τ is the torsion, $\mathbf{T}$ the tangent, $\mathbf{N}$ the normal, and $\mathbf{B}$ the binormal vector of $\mathbf{a}$.

Notice that now the construction is based on the rigid motion of $\mathbf{a}$, not on a curve γ on the envelope as before. If $\mathbf{a}$ is given, then R is completely specified, so there are two degrees of freedom to choose the motion E.

Proof. We can assume that $\mathbf{a}$ is parameterized by arc-length. We denote by $\mathbf{y}_0$ and $\mathbf{y}_1$ the points on the characteristic curves at height 0, so $y_{0,3} = y_{1,3} = 0$. From Eq. (14) we see that $\mathbf{T} \cdot R\mathbf{y}_i = 0$, so there are two alternatives: (i) $R^{-1}\mathbf{T} = \mathbf{e}_3$ or (ii) $R^{-1}\mathbf{T} \neq \mathbf{e}_3$. The case (i) implies that $\mathbf{T} = R\mathbf{e}_3$, so it remains to analyze the other case.

If $R^{-1}\mathbf{T} \neq \mathbf{e}_3$ then $\mathbf{y}_0 = -\mathbf{y}_1$, which in turn implies, by the second identity in Eq. (14), that $\mathbf{T} \cdot R\mathbf{e}_3 = 0$ and $\mathbf{T} = \lambda \frac{d}{dt}R\mathbf{e}_3$ for some $\lambda \in \mathbb{R}$. The former implies that

$$R\mathbf{e}_3 = A_1\mathbf{N} + A_2\mathbf{B}$$

for some pair of functions A_1 and A_2. Taking derivatives and using the Frenet–Serret formulas we have

$$\tfrac{d}{dt}R\mathbf{e}_3 = -A_1\kappa\mathbf{T} + (\tfrac{d}{dt}A_1 - A_2\tau)\mathbf{N} + (\tfrac{d}{dt}A_2 + A_1\tau)\mathbf{B}.$$

Since $\mathbf{T} = \lambda\frac{d}{dt}R\mathbf{e}_3$, then

$$\tfrac{d}{dt}A_1 = \tau A_2 \qquad \text{and} \qquad \tfrac{d}{dt}A_2 = -\tau A_1.$$

If we define $z = A_1 + iA_2$, then the differential equations can be written as $\frac{d}{dt}z = -\tau iz$, and they possess a solution $z = \exp(-i(\int \tau + c))$, for some constant c, which concludes the analysis of case (ii). $\qquad\square$

Observe that Theorem 12 is redundant from the point of view of any machining application as the continuity of the "upper" envelope is irrelevant; however, it shows that generically such a motion exist and is locally uniquely determined, once the instantaneous velocity vector of one axis point is given. The geometric argument for the uniqueness comes from the fact that the continuity of the envelope at $\mathbf{x}_0^2$ gives another linear constraint (another plane in Fig. 13) that would result in (generically) a single intersection point, and consequently the instantaneous velocity vector of the center of the sphere S_- in Fig. 13(a).

Remark 3. *In general, to preserve the continuity of the envelope when the tool is not C^1 continuous at two points, then the family of motions reduces to two degrees of freedom. Recall also a special case with an arbitrary number of points where the tool is C^1-discontinuous, in which case pure translations perpendicular to the main axis always generate C^0 continuous envelopes.*

4.3 Examples

We now show several results on motion design of (at least) C^1 continuous tools with a single point of C^0 continuity.

Example 5. *To demonstrate the degrees of freedom for a motion design of a particular C^0 continuous tool, we fix the tool axis and the instantaneous velocity vector at one endpoint of the axis. Since one can assume a normalized velocity vector, this gives two degrees of freedom. Based on the results of Theorem 12, one has a one-parameter family of endpoints for the instantaneous velocity vector at the other endpoint of the axis to make the resulting envelope C^0 continuous. In this example, we use a tool where the radii of the inscribed spheres are given by two symmetric cubic radial functions that create a sharp edge (circle) on the tool*

$$r_1(s) = \frac{241s^3}{32} - \frac{369s^2}{32} - 3s + 14, \quad r_2(s) = -\frac{241s^3}{32} + \frac{177s^2}{16} + \frac{111s}{32} + 8.$$
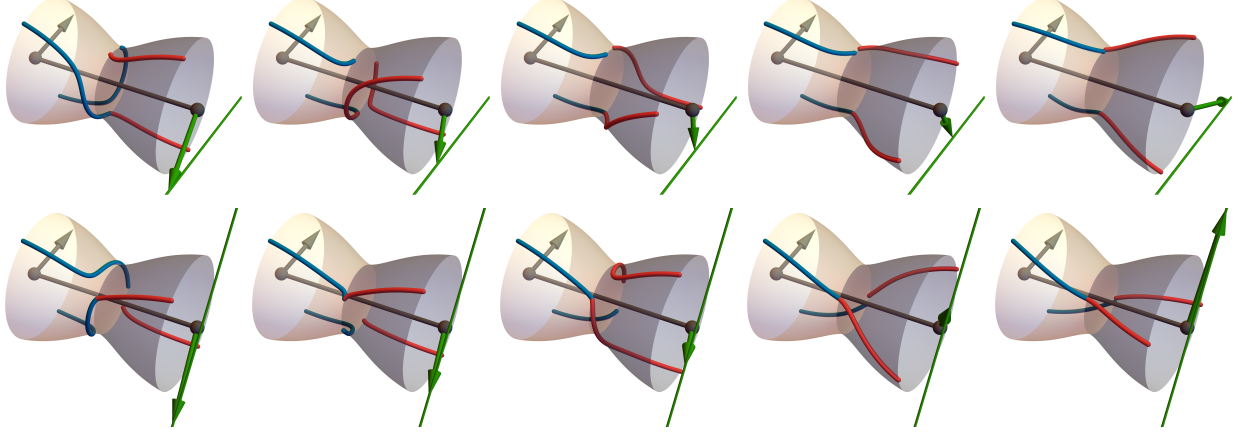
Figure 16: Three degrees of freedom to move a C^0 continuous tool such that the resulting envelope is also C^0 continuous. For a fixed position of the tool and an instantaneous velocity vector at the left endpoint (two degrees of freedom), the endpoint of the velocity vector (green) at the other endpoint of the axis has to lie on the green line (third degree of freedom). Two solution sets are shown, depending on which point the characteristics (red and blue) are forced to meet the C^0 continuity constraint.

The length of the tool axis is 40 *and is aligned with the x-axis. The velocity vector is uniquely given (up to a scalar multiple) by two boundary velocity vectors. We set*

$$\mathbf{v}_1 = (20, 90, 40).$$

The requirement of C^0 continuity of a branch of the characteristic yields two 1-parametric families of solutions for $\mathbf{v}_2$, i.e,

$$\mathbf{v}_2^{\pm} = \left(20, s, \pm\frac{4\left(60\sqrt{1951}s - 2223s + 5400\sqrt{1951} - 64000\right)}{13607}\right).$$

The solution is demonstrated in Fig. 16 (and the attached video).

With three degrees of freedom one can, in the path-planning stage, essentially prescribe the motion of one point of the axis and then still has one degree of freedom left to maneuver the tool. This is demonstrated in the next example.

Example 6. *Consider the following trajectory of one end point of the tool axis*[3]

$$\mathbf{a}(t) = \left(2t + 1, 200t, 16t^2 - 16t + 4\right),$$

see Fig. 17. Therefore, at each instant, we already have a boundary velocity vector $\mathbf{v}_1 = \mathbf{a}'(t)$. If we aim for a motion with one continuous branch of the characteristic, we have one degree

---

[3]It is convenient to choose a boundary point of the axis, but one can choose any other point as well.
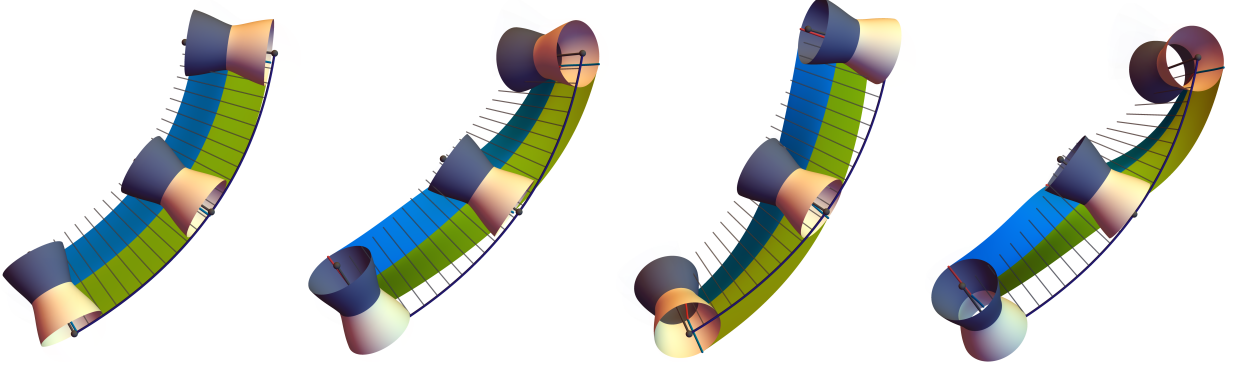
Figure 17: A family of motions with fixed one rail curve of a C^0 continuous tool producing C^0 continuous envelope strips (green and blue). At each time instant, one has a one-parameter family of admissible positions of the tool.

of freedom to choose the tool axis direction, and thus the second boundary velocity vector at each instant. More specifically, the axis direction can be described as

$$\mathbf{l}(t) = \left(\frac{2u(t)}{u(t)^2 + v(t)^2 + 1}, \frac{2v(t)}{u(t)^2 + v(t)^2 + 1}, \frac{u(t)^2 + v(t)^2 - 1}{u(t)^2 + v(t)^2 + 1} \right)$$

for some real functions $u(t), v(t) \in \mathbb{R}(t)$. Then the computation of the admissible axis directions leads to the solution of ordinary differential equations; recall Eq. (14). In our implementation, we compute the tool motion (described by the two rail curves) as fine polylines obtained by integrating a boundary velocity vectors at each time instance. More precisely, we start with a rail (boundary curve) $\mathbf{a}(t)$ (which gives $\mathbf{v}_1(t)$) and a certain position of the tool axis $\mathbf{l}$ at $t = 0$, which gives the position of the second boundary point $\mathbf{b}(0)$. Then we choose a solution $\mathbf{v}_2(0)$ from all possible velocity vectors at $\mathbf{b}(0)$. Once we have the instantaneous motion, we can move the tool accordingly and repeat the process. Note that the situation is similar to the case when we prescribe a motion of a left/right sphere inscribed in the C^0 continuity point; recall Fig. 13(a). There, we also have a one-parameter family of instantaneous motions at each time instant.

The three degrees of freedom can be exploited for motion design that moves the tool tangentially to the given reference surface. This is shown in our last example.

Example 7. *Consider a reference surface Φ with a cuspidal curve; see Fig. 18. The surface can be either convex or concave in the neighborhood of the curve. With a proper tool that complements the geometry of the surface, that is, a convex tool for a concave surface and vice versa, we can move the tool tangentially to Φ at one point, while gliding the surface with the C^0 continuous tool along the cuspidal curve. Note that we would need to do two paths; there are not enough degrees of freedom to preserve the tangential contact at two points, and also glide the tool along the cuspidal curve.*
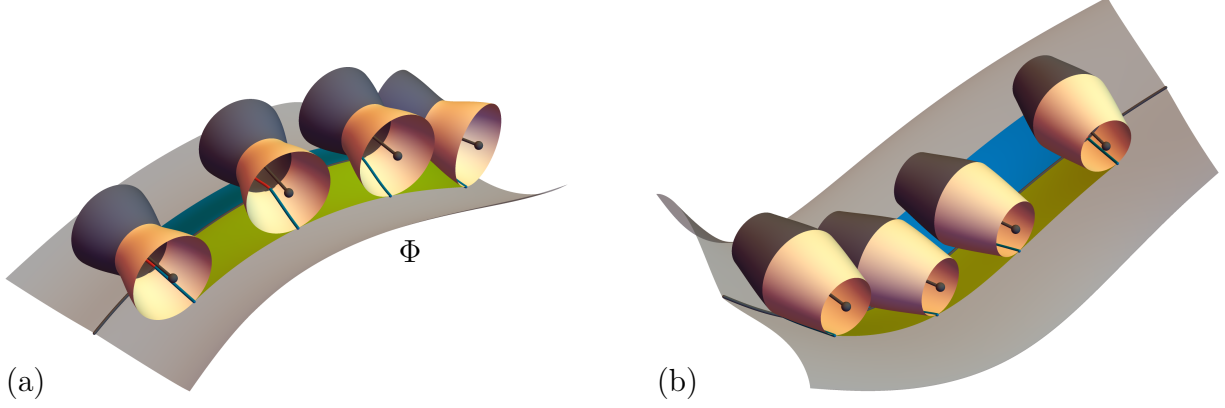
Figure 18: Using a C^0 continuous tool for machining a special target surface Φ with a cuspidal curve.

5 Conclusion

We have studied the envelopes of rotational rigid bodies whose motions and profile curve possess decreased regularity. In particular, we have proven that C^1 continuous bodies and C^1 continuous motions result in C^1 continuous envelopes. In the case of solids with meridians containing one point of C^0 continuity, we have shown that one can still generate motions that produce C^0 envelopes, and we have classified a three-parametric family of such motions. We believe that the problem of smoothness of envelopes deserves more attention; for example, how does the local structure of envelopes depend on the smoothness of tool and motion? Can we find conditions that ensure that the envelope is C^1 continuous locally even when the tool or motion are not C^2 continuous everywhere? Our work is a first step on the study of these questions. We have demonstrated our theoretical results in motion design in the context of 5-axis CNC machining, where tools with C^0 continuities frequently occur.

As a future thread for research, we aim at curve slot milling of free-form surfaces with sharp edges (cuspidal curves). While the motion design with a fixed tool is limited in terms of degrees of freedom, one may look also at optimal shape of the tool that would comfort the given free-form geometry. Another related issue is on detection and prevention of self-intersections. In the current setup, the envelopes may contain self-intersections, which from the machining perspective is highly undesirable. One can employ self-intersection algorithms, e.g. [13], as a post-processing to check that the constructed envelopes are self-intersection free. However, incorporating some sufficient conditions on the construction of self-intersection free motions directly into the envelope construction offers a challenging direction for a future research.

Acknowledgments

discontinuity of the envelope in Remark 2 is thanks to one of the reviewers.

Funding

References

[1] Bharat Adsul, Jinesh Machchhar, and Milind Sohoni. Local and global analysis of parametric solid sweeps. *Computer Aided Geometric Design*, 31(6):294–316, 2014.

[2] John A. Baker. Plane curves, polar coordinates and winding numbers. *Math. Mag.*, 64(2):75–91, 1991.

[3] M. Bartoň, M. Bizzarri, F. Rist, O. Sliusarenko, and H. Pottmann. Geometry and tool motion planning for curvature adapted CNC machining. *ACM Trans. Graph.*, 40(4):1–16, 2021.

[4] Denis Blackmore, Roman Samulyak, and Ming C. Leu. Trimming swept volumes. *Computer-Aided Design*, 31(3):215–223, 1999.

[5] Pengbo Bo and Michael Bartoň. On initialization of milling paths for 5-axis flank CNC machining of free-form surfaces with general milling tools. *Computer Aided Geometric Design*, 71:30–42, 2019.

[6] G. Elber and R. Fish. 5-axis freeform surface milling using piecewise ruled surface approximation. *ASME Journal of Manufacturing Science and Engineering*, 119(3):383–387, 1997.

[7] Hüseyin Erdim and Horea T. Ilieş. Detecting and quantifying envelope singularities in the plane. *Computer-Aided Design*, 39(10):829–840, 2007.

[8] Ali Hashemian, Pengbo Bo, and Michael Bartoň. Reparameterization of ruled surfaces: toward generating smooth jerk-minimized toolpaths for multi-axis flank CNC milling. *Computer-Aided Design*, 127:102868, 2020.

[9] Erwin Kreyszig. *Differential geometry*. Dover Publications, Inc., New York, 1991. Reprint of the 1963 edition.

[10] Seok Won Lee and Andreas Nestler. Complete swept volume generation, part I: Swept volume of a piecewise C^1-continuous cutter at five-axis milling via gauss map. *Computer-Aided Design*, 43(4):427–441, 2011.

[11] Seok Won Lee and Andreas Nestler. Complete swept volume generation, part II: NC simulation of self-penetration via comprehensive analysis of envelope profiles. *Computer-Aided Design*, 43(4):442–456, 2011.

[12] C. Li, S. Bedi, and S. Mann. Flank millable surface design with conical and barrel tools. *Computer- Aided Design and Applications*, 5:461–470, 2008.

[13] Diana Pekerman, Gershon Elber, and Myung-Soo Kim. Self-intersection detection and elimination in freeform curves and surfaces. *Computer-Aided Design*, 40(2):150–159, 2008.

[14] H. Pottmann and J. Wallner. *Computational Line Geometry*. Springer, Heidelberg, 2001.

[15] D. Roth, S. Bedi, F. Ismail, and S. Mann. Surface swept by a toroidal cutter during 5-axis machining. *Computer-Aided Design*, 33(1):57–63, 2001.

[16] C.C.L. Wang and G. Elber. Multi-dimensional dynamic programming in ruled surface fitting. *Computer-Aided Design*, 51:39–49, 2014.

[17] C.C.L. Wang and K. Tang. Optimal boundary triangulations of an interpolating ruled surface. *Journal of Computing and Information Science in Engineering*, 5(4):291–301, 2005.

[18] G. Zheng, Q.-Z. Bi, and L.-M. Zhu. Smooth tool path generation for five-axis flank milling using multi-objective programming. In *Proceedings of the Institution of Mechanical Engineers, Part B: Journal of Engineering Manufacture*, volume 226, pages 247–254, 2012.

[19] LiMin Zhu and YaoAn Lu. Geometric conditions for tangent continuity of swept tool envelopes with application to multi-pass flank milling. *Computer-Aided Design*, 59:43–49, 2015.

[20] LiMin Zhu, Gang Zheng, and Han Ding. Formulating the swept envelope of rotary cutter undergoing general spatial motion for multi-axis NC machining. *International Journal of Machine Tools and Manufacture*, 49(2):199–202, 2009.